

RESEARCH ARTICLE | JULY 17 2023

Jacobian-free variational method for computing connecting orbits in nonlinear dynamical systems

Omid Ashtari  ; Tobias M. Schneider  




Chaos 33, 073134 (2023)

<https://doi.org/10.1063/5.0143923>




CrossMark



Chaos

Special Topic: Nonautonomous Dynamics
in the Climate Sciences

Submit Today

 AIP
Publishing

Jacobian-free variational method for computing connecting orbits in nonlinear dynamical systems

Cite as: Chaos 33, 073134 (2023); doi: 10.1063/5.0143923

Submitted: 27 January 2023 · Accepted: 24 June 2023 ·

Published Online: 17 July 2023



View Online



Export Citation



CrossMark

Omid Ashtari¹ and Tobias M. Schneider^{a)}

AFFILIATIONS

Emergent Complexity in Physical Systems Laboratory (ECPS), École Polytechnique Fédérale de Lausanne (EPFL), CH-1015 Lausanne, Switzerland

^{a)} Author to whom correspondence should be addressed: tobias.schneider@epfl.ch

ABSTRACT

One approach for describing spatiotemporal chaos is to study the unstable invariant sets embedded in the chaotic attractor of the system. While equilibria, periodic orbits, and invariant tori can be computed using existing methods, the numerical identification of heteroclinic and homoclinic connections between them remains challenging. We propose a robust matrix-free variational method for computing connecting orbits between equilibrium solutions. Instead of a common shooting-based approach, we view the identification of a connecting orbit as a minimization problem in the space of smooth curves in the state space that connect the two equilibria. In this approach, the deviation of a connecting curve from an integral curve of the vector field is penalized by a non-negative cost function. Minimization of the cost function deforms a trial curve until, at a global minimum, a connecting orbit is obtained. The method has no limitation on the dimension of the unstable manifold at the origin equilibrium and does not suffer from exponential error amplification associated with time-marching a chaotic system. Owing to adjoint-based minimization techniques, no Jacobian matrices need to be constructed. Therefore, the memory requirement scales linearly with the size of the problem, allowing the method to be applied to high-dimensional dynamical systems. The robustness of the method is demonstrated for the one-dimensional Kuramoto–Sivashinsky equation.

© 2023 Author(s). All article content, except where otherwise noted, is licensed under a Creative Commons Attribution (CC BY) license (<http://creativecommons.org/licenses/by/4.0/>). <https://doi.org/10.1063/5.0143923>

The chaotic evolution of a dynamical system can be described in terms of the non-chaotic unstable invariant solutions embedded within its chaotic attractor. Heteroclinic and homoclinic orbits between these invariant solutions mediate the evolution of the chaotic trajectory from the vicinity of one invariant solution to the vicinity of another one. Despite their importance for a complete dynamical description of the chaotic dynamics, the identification of connecting orbits has remained a computational challenge. We introduce a robust and memory-efficient method for computing connecting orbits between equilibrium solutions.

I. INTRODUCTION

A broad spectrum of physical systems, from fluid flows¹ to nonlinear optics^{2,3} and suspensions of motile micro-organisms,^{4,5} exhibit spatiotemporally chaotic dynamics. In the framework of dynamical systems, the spatiotemporal chaos is viewed as the evolution of a chaotic trajectory in the state space of the governing equations.

Embedded in the state space are non-chaotic, time-invariant solutions including equilibria, periodic orbits, and invariant tori. These invariant solutions are dynamically unstable so that the chaotic trajectory visits them transiently, yet recurrently. Spatiotemporal chaos can, thus, be viewed as a walk through a forest of invariant solutions that form the elementary building blocks of the chaotic solution.^{6–8} Consequently, individual invariant solutions are able to capture essential properties of the observed spatiotemporal structures, and, collectively, they promise an avenue toward quantitatively predicting statistical properties of the chaotic dynamics. The increasing computational resources and algorithmic advances have enabled these concepts, originally developed in the context of low-dimensional chaotic dynamical systems, to be applied to high-dimensional problems including transitional turbulence where descriptions based on invariant solutions have proven to be particularly useful.^{9–14}

While equilibria and periodic orbits form the building blocks of the dynamics, the chaotic evolution from the neighborhood of one unstable invariant solution to another is mediated by *connecting*

orbits. These hetero- and homoclinic connections provide dynamic pathways between different periodic orbits or equilibria within the chaotic attractor. Therefore, a complete dynamical description of the chaotic dynamics in terms of state-space structures requires to both identify equilibria, periodic orbits, and invariant tori embedded in the chaotic attractor and compute connecting orbits between them. In the context of fluid dynamics, for example, Kawahara and Kida¹⁵ and van Veen and Kawahara¹⁶ use connecting orbits to explain the turbulent bursting in plane Couette flow; Suri *et al.* study the network of connecting orbits that underpins the transient dynamics in a quasi-two-dimensional Kolmogorov flow;¹⁷ Reetz and Schneider characterize the time-dependent dynamics of inclined layer convection using connecting orbits between coexisting invariant solutions;¹⁸ and De Jesús and Graham discuss a network of dynamically connected relative periodic orbits that organizes the attractor in a two-dimensional Kolmogorov flow.¹⁹

We specifically focus on connecting orbits between equilibrium solutions. Such connecting orbits have been identified as dynamically relevant in fluid systems,^{17,18,20} and they are involved in global bifurcations when, for instance, a periodic orbit bifurcates off a homoclinic orbit or a heteroclinic cycle.^{21,22} Connecting orbits are located within the intersection of the unstable manifold of one equilibrium with the stable manifold of another or the same equilibrium solution if they are of heteroclinic or homoclinic type, respectively. In the vicinity of an equilibrium solution, a trajectory approaches/departs the equilibrium along its stable/unstable manifold exponentially in time. Consequently, the time required to traverse the entire connecting orbit is not finite. This infinite passage time makes computing connecting orbits very challenging.

One approach to handle the computational challenge of the infinite passage time is to truncate the connecting orbit and compute part of the orbit that is traversed in finite time. Under favorable conditions, the truncated orbit can be computed using shooting methods. Geometrically, the truncation approach searches for an initial condition on the unstable manifold of the origin equilibrium whose resulting trajectory lands on the stable manifold of the destination equilibrium. Due to their curvature, parametrizations of stable and unstable manifolds are usually not accessible. Consequently, they need to be approximated locally by the corresponding tangent spaces associated with the origin and destination equilibrium. Practically, a connecting orbit is, thus, approximated by identifying an initial condition in the intersection of the unstable tangent space of and a hypersphere around the origin equilibrium, which after forward time integration reaches a distance below a chosen threshold from the destination equilibrium.²³ If the hypersphere is chosen small enough, the unstable tangent space accurately approximates the unstable manifold, and thus, the obtained trajectory accurately represents a connecting orbit.

Even if the unstable manifold can be accurately approximated by the unstable tangent space, a systematic search for an initial condition that eventually reaches the destination equilibrium is a formidable task, especially for a chaotic system where nearby trajectories diverge exponentially with time. When the unstable manifold at the origin equilibrium solution is two-dimensional, an exhaustive search strategy can be employed.^{11,17,24,25} In this case, the search space is a circle on the unstable tangent space with an angle being the only variable. However, when the unstable tangent space at the

origin equilibrium has more than two dimensions, the search space is too large for an exhaustive search. To improve the dimensionality drawback, Farano *et al.*²⁶ propose an adjoint-based variational method for finding a state on an energy shell around the origin equilibrium whose trajectory reaches another energy shell around the destination equilibrium. They do not constrain the initial condition to be located on the unstable tangent space at the origin equilibrium, hence as a second step, the trajectory is confirmed to shadow a connecting orbit by matching the end points of the trajectory against the linearized dynamics around the two equilibria. In all these methods determining the size of the hypersphere around the origin equilibrium solution is not a trivial task: the hypersphere should be small enough in order for the tangent space to accurately approximate the manifold, and large enough to let the required time integration intervals be feasibly short.

An alternative to the shooting-based methods, which search for a single state on the connecting orbit, is to search in the space of *connecting curves*, i.e., all smooth curves in the state space which connect the two equilibria. Among all such curves, only connecting orbits are integral curves of the vector field induced by the governing equation. The idea is to start from a connecting curve pivoted on the two fixed points, then deform the curve until the tangent velocity coincides with the local field vector along the entire curve, and thus, a connecting orbit is achieved. This approach has several advantages over the reviewed shooting-based methods for computing connecting orbits: First, there is no limitation on the dimensionality of the unstable manifold at the origin equilibrium because no exhaustive search is needed; Second, the approach does not suffer from the exponential separation of trajectories with time since the connecting curve is deformed locally and no time integration is required; and finally, this approach yields the exact and the entire connecting orbit without requiring to truncate it.

Despite the conceptual advantages of searching in the space of connecting curves over the shooting-based alternatives, this approach is not extensively developed on the practical side. Liu *et al.*²⁷ use rational Chebyshev basis functions for the spectral representation of variables along the infinite temporal direction probably for the first time in this context. They formulate the problem as a system of nonlinear equations by setting the temporal derivative equal to the right-hand side of the governing equation for every state variable at every temporal collocation point. They then solve the resulting system of equations using standard Newton iterations. Dong and Lan²⁸ extend the variational method of Lan and Cvitanović,²⁹ originally developed for finding periodic orbits, to the problem of computing connecting orbits. They view the problem of deforming connecting curves toward a connecting orbit as a minimization problem: a connecting orbit is found by minimizing a cost function, which penalizes the deviation of a connecting curve from being an integral curve of the vector field. They employ an infinitesimal-step version of Newton iterations for continuously deforming the curve and use finite differences for calculating the tangent velocity vector. In his Ph.D. thesis, Pallantla³⁰ employs the same spectral representation of variables in the temporal direction as in Ref. 27 and deforms the curve in the direction of the steepest descent of the cost function. The common drawback of the aforementioned algorithms is that they all require explicit construction of the Jacobian matrix. In a system with M temporal and N spatial degrees of

freedom, the size of the Jacobian matrix scales as $\mathcal{O}(M^2N^2)$, which can be prohibitively large for high-dimensional dynamical systems such as three-dimensional fluid flows.

In order to transfer the advantages of searching in the space of connecting curves to high-dimensional dynamical systems, we propose a Jacobian-free variational method for computing connecting orbits between two equilibrium solutions. The method employs an adjoint-based optimization technique to minimize a cost function, which measures the deviation of a connecting curve between two equilibria from an integral curve of the vector field. We construct a globally contracting dynamical system in the space of connecting curves. Fixed points of this dynamical system are minima of the non-negative cost function. The global minima of the cost function, taking zero value, correspond to connecting orbits of the original dynamical system. Therefore, connecting orbits are found by integrating the dynamics in the space of connecting curves. Due to the explicit construction of the dynamical system in the space of connecting curves, the memory requirement scales as $\mathcal{O}(MN)$ which allows the proposed method to be applied to high-dimensional dynamical systems.

The remainder of the present article is organized as follows. In Sec. II, the problem of computing a connecting orbit is set up as a minimization problem, and in Sec. III, the adjoint-based minimization technique is formulated for a general autonomous dynamical system. In Sec. IV, a spectral representation suitable for the discretization along the unbounded temporal domain is discussed. To demonstrate the robustness of the proposed variational method, in Sec. V, we consider the one-dimensional Kuramoto–Sivashinsky equation in a spatiotemporally chaotic regime and show that several connecting orbits can be converged reliably. Finally, in Sec. VI, the paper is summarized and an outlook for future research is given.

II. VARIATIONAL METHOD FOR FINDING CONNECTING ORBITS

We consider general autonomous dynamical systems of the form

$$\frac{\partial \mathbf{u}}{\partial t} = \mathbf{f}(\mathbf{u}), \quad (1)$$

where the smooth nonlinear operator \mathbf{f} governs the evolution of an n -dimensional real field $\mathbf{u} \in \mathcal{M} \subset \mathbb{R}^n$ defined over a d -dimensional spatial domain $\mathbf{x} \in \Omega \subset \mathbb{R}^d$ and time $t \in \mathbb{R}$ subject to time-independent boundary conditions (BCs) at $\partial\Omega$, the boundaries of the spatial domain Ω .

A connecting orbit between two equilibrium solutions is a solution trajectory $\mathbf{u}(\mathbf{x}, t)$ of the governing equation (1) such that the asymptotic conditions

$$\lim_{t \rightarrow -\infty} \mathbf{u} = \mathbf{u}_-, \quad \lim_{t \rightarrow +\infty} \mathbf{u} = \mathbf{u}_+, \quad \mathbf{f}(\mathbf{u}_{\pm}) = \mathbf{0} \quad (2)$$

are satisfied in the temporal direction. The connecting orbit is a heteroclinic connection if $\mathbf{u}_- \neq \mathbf{u}_+$ and a homoclinic connection if $\mathbf{u}_- = \mathbf{u}_+$ (while implicitly assuming that the entire orbit is not the equilibrium solution itself.)

In the $(d + 1)$ -dimensional space-time domain of the dynamical system (1), connecting orbits are solutions to a boundary value problem subject to the same BCs as Eq. (1) in d spatial directions,

augmented by the asymptotic BCs (2) in the temporal direction. The idea of the proposed variational method is to consider C^∞ space-time fields that satisfy the boundary conditions in all $(d+1)$ directions and vary the field until Eq. (1) is satisfied at each and every space-time coordinate. Geometrically, $\mathbf{f}(\mathbf{u})$ is a vector field in the n -dimensional state space \mathcal{M} , \mathbf{u}_- and \mathbf{u}_+ are two fixed points, and connecting orbits are integral curves of this vector field extending from \mathbf{u}_- to \mathbf{u}_+ . In this picture, the search space is the space of all smooth curves in the state space that connect the two fixed points. We define the space of connecting curves, denoted by \mathcal{C}_g , as

$$\mathcal{C}_g = \left\{ \mathbf{u}(\mathbf{x}, s) \left| \begin{array}{l} \mathbf{u} : \Omega \times \mathbb{R} \rightarrow \mathcal{M} \\ \lim_{s \rightarrow \pm\infty} \mathbf{u} = \mathbf{u}_{\pm} \\ \mathbf{u} \text{ satisfies BCs at } \partial\Omega \end{array} \right. \right\}. \quad (3)$$

We parameterize connecting curves by $s \in \mathbb{R}$ in order to distinguish the evolution along a connecting curve from the evolution along a solution trajectory of the governing equation (1), which is parameterized by the physical time t . Connecting orbits form a subset $\mathcal{C} \subset \mathcal{C}_g$ in which the tangent velocity vector, $\partial \mathbf{u} / \partial s$, coincides with the local field vector, $\partial \mathbf{u} / \partial t = \mathbf{f}(\mathbf{u})$, along the entire connecting curve. As a measure of deviation of a connecting curve from being a connecting orbit, we define the non-negative cost function J^2 as

$$J^2 = \int_{-\infty}^{+\infty} \int_{\Omega} \mathbf{r} \cdot \mathbf{r} \, dx ds, \quad (4)$$

where \mathbf{r} is the local deviation of the tangent velocity vector from the field vector, or the residual of Eq. (1)

$$\mathbf{r}(\mathbf{u}) = \mathbf{f}(\mathbf{u}) - \frac{\partial \mathbf{u}}{\partial s} \quad (5)$$

and \cdot indicates the standard Euclidean inner product. The residual \mathbf{r} is zero everywhere along a connecting orbit. Therefore, the cost function takes zero value for $\mathbf{u} \in \mathcal{C}$, while it takes a positive value for $\mathbf{u} \in \mathcal{C}_g \setminus \mathcal{C}$. The problem of finding connecting orbits can now

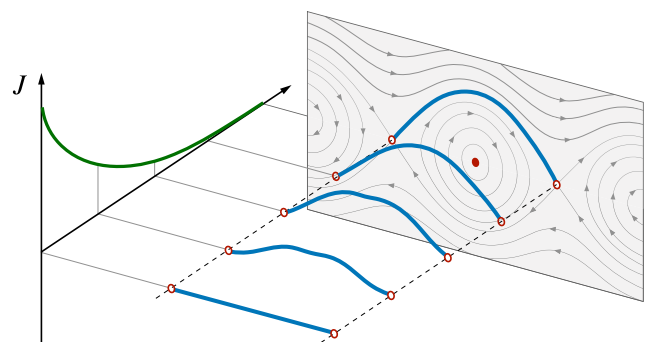


FIG. 1. Schematic of the variational method for computing a connecting orbit between two equilibrium solutions: A connecting curve pivoted on the two fixed points is deformed such that a cost function J measuring the deviation of the connecting curve from being an integral curve of the vector field is minimized. For a connecting orbit, the tangent velocity vector matches the field vector along the entire curve and, thus, the global minimum of the cost function, $J = 0$, is achieved.

be viewed as a minimization problem in \mathcal{C}_g : Absolute minima of J^2 , for which $J = 0$, correspond to connecting orbits $\mathbf{u} \in \mathcal{C}$. Figure 1 schematically shows the idea of this approach: Minimizing the cost function J deforms a curve connecting two fixed points of the vector field toward an integral curve of the vector field bounded between the two equilibria, thereby a connecting orbit.

III. ADJOINT-BASED MINIMIZATION OF THE COST FUNCTION

We have recast the problem of computing connecting orbits into a minimization problem in the space of connecting curves extended between two equilibrium solutions. Absolute minima of the non-negative cost function J^2 with $J = 0$ correspond to a connecting orbit. To solve the minimization problem, we employ an adjoint-based technique inspired by the recent works of Farazmand³¹ on identifying equilibria and traveling waves and Azimi *et al.*³² on computing periodic orbits of nonlinear dynamical systems. We construct a dynamical system in the space of connecting curves, \mathcal{C}_g , such that along its trajectories the cost function is guaranteed to decrease monotonically. Therefore, connecting orbits are found by integrating the constructed dynamics in \mathcal{C}_g until a minimum of the cost function is reached. Parametrizing this dynamical system by a fictitious time τ , we need to construct the operator $\mathbf{G}(\mathbf{u})$ such that evolution of \mathbf{u} governed by

$$\frac{\partial \mathbf{u}}{\partial \tau} = \mathbf{G}(\mathbf{u}) \quad (6)$$

guarantees

$$\frac{\partial J^2}{\partial \tau} \leq 0, \quad \forall \tau. \quad (7)$$

We define the inner product space $\mathcal{C}_s \supset \mathcal{C}_g$

$$\mathcal{C}_s = \left\{ \mathbf{q}(\mathbf{x}, s) \mid \begin{array}{l} \mathbf{q} : \Omega \times \mathbb{R} \rightarrow \mathbb{R}^n \\ \lim_{s \rightarrow \pm\infty} \mathbf{q} = \mathbf{v}_{\pm} \in \mathbb{R}^n \end{array} \right\} \quad (8)$$

together with the real-valued inner product

$$\begin{aligned} \langle \cdot, \cdot \rangle : \mathcal{C}_s \times \mathcal{C}_s &\rightarrow \mathbb{R}, \\ \langle \mathbf{q}_1, \mathbf{q}_2 \rangle &= \int_{-\infty}^{+\infty} \int_{\Omega} \mathbf{q}_1 \cdot \mathbf{q}_2 \, d\mathbf{x} \, ds, \end{aligned} \quad (9)$$

and L_2 -norm

$$\|\mathbf{q}\| = \sqrt{\langle \mathbf{q}, \mathbf{q} \rangle}. \quad (10)$$

In contrast to the space of connecting curves \mathcal{C}_g , the elements of \mathcal{C}_s have arbitrary asymptotic states $\mathbf{v}_{\pm} \in \mathbb{R}^n$. The rate of change of the cost function $J^2 = \|\mathbf{r}\|^2 = \langle \mathbf{r}, \mathbf{r} \rangle$ is obtained by the inner product of $\mathbf{r}(\mathbf{u})$ with its directional derivative along the to-be-determined operator $\partial \mathbf{u} / \partial \tau = \mathbf{G}(\mathbf{u})$,

$$\frac{\partial J^2}{\partial \tau} = 2 \left\langle \left(\nabla_{\mathbf{u}} \mathbf{r} \right) \frac{\partial \mathbf{u}}{\partial \tau}, \mathbf{r} \right\rangle. \quad (11)$$

The directional derivative of $\mathbf{r}(\mathbf{u})$ along \mathbf{G} is defined as

$$\mathcal{L}(\mathbf{u}; \mathbf{G}) = \lim_{\varepsilon \rightarrow 0} \frac{\mathbf{r}(\mathbf{u} + \varepsilon \mathbf{G}) - \mathbf{r}(\mathbf{u})}{\varepsilon}. \quad (12)$$

Using the adjoint of the directional derivative, we can write Eq. (11) as

$$\frac{\partial J^2}{\partial \tau} = 2 \langle \mathcal{L}^\dagger(\mathbf{u}; \mathbf{r}), \mathbf{G} \rangle, \quad (13)$$

where \mathcal{L}^\dagger is the adjoint operator of \mathcal{L} , with

$$\langle \mathcal{L}(\mathbf{u}; \mathbf{G}), \mathbf{r} \rangle = \langle \mathbf{G}, \mathcal{L}^\dagger(\mathbf{u}; \mathbf{r}) \rangle, \quad (14)$$

for all connecting curves $\mathbf{u} \in \mathcal{C}_g$. The residual \mathbf{r} [defined in Eq. (5)] and the operator \mathbf{G} [defined in Eq. (6)] are functions of \mathbf{u} and belong to the inner product space \mathcal{C}_s with certain properties that are detailed shortly. By choosing $\mathbf{G}(\mathbf{u}) = -\mathcal{L}^\dagger(\mathbf{u}; \mathbf{r})$, the monotonic decrease of the cost function is guaranteed,

$$\frac{\partial J^2}{\partial \tau} = 2 \langle \mathcal{L}^\dagger(\mathbf{u}; \mathbf{r}), -\mathcal{L}^\dagger(\mathbf{u}; \mathbf{r}) \rangle = -2 \|\mathcal{L}^\dagger(\mathbf{u}; \mathbf{r})\|^2 \leq 0. \quad (15)$$

The dynamical system $\partial \mathbf{u} / \partial \tau = \mathbf{G}(\mathbf{u}) = -\mathcal{L}^\dagger(\mathbf{u}; \mathbf{r})$ is globally contracting. All trajectories are eventually attracted to stable fixed points at which $\partial \mathbf{u} / \partial \tau = \mathbf{0}$ and J^2 takes a minimum value. Although the monotonic decrease of the cost function is guaranteed along trajectories of the dynamics in \mathcal{C}_g , reaching the global minimum is not. To find a connecting orbit, therefore, the dynamics in the space of connecting curves is integrated until a fixed point is reached. Those fixed points of $\partial \mathbf{u} / \partial \tau = \mathbf{G}(\mathbf{u})$, which correspond to the global minimum of the cost function, $J = 0$, are connecting orbits of the original dynamical system $\partial \mathbf{u} / \partial t = \mathbf{f}(\mathbf{u})$, and those corresponding to $J > 0$ are rejected.

The dynamical system $\partial \mathbf{u} / \partial \tau = \mathbf{G}(\mathbf{u})$ is constructed in the space of connecting curves \mathcal{C}_g defined in Eq. (3). This imposes certain BCs on the residual $\mathbf{r}(\mathbf{u})$ and the operator $\mathbf{G}(\mathbf{u})$. In the temporal direction, $\lim_{s \rightarrow \pm\infty} \mathbf{r} = \mathbf{0}$ since \mathbf{u} satisfies the correct asymptotic BCs for all τ , and $\lim_{s \rightarrow \pm\infty} \mathbf{G} = \mathbf{0}$ since the correct asymptotic values of \mathbf{u} must be preserved. In space, \mathbf{u} satisfies the correct BCs at $\partial \Omega$ for all τ ; consequently, the spatial BCs of \mathbf{r} and \mathbf{G} are determined following similar arguments. For example, \mathbf{r} and \mathbf{G} will be periodic in directions where \mathbf{u} is periodic, will take zero value at the boundaries where \mathbf{u} satisfies Dirichlet boundary conditions and so forth. These properties must be taken into account while deriving the adjoint operator from the definition (14). Derivation of the adjoint operator for the Kuramoto–Sivashinsky system, introduced in Sec. V, is presented in Appendix A where the zero asymptotic values of \mathbf{r} and \mathbf{G} in the temporal direction and their periodicity in space enable us to derive the adjoint operator as an explicit function of the space–time field \mathbf{u} .

Both heteroclinic and homoclinic connections can be numerically identified using the introduced variational method. In the case of a homoclinic connection to an equilibrium solution, zero variation in time, i.e., the equilibrium solution itself, is a trivial solution satisfying the definition (2). Therefore, depending on the initial connecting curve from which the integration starts, a trivial or a nontrivial solution with $J = 0$ can be obtained. The definition of a heteroclinic connection does not have any trivial solution.

On an abstract level, we construct the operator \mathbf{G} following the same logic as that employed by Farazmand³¹ in computing equilibria and by Azimi *et al.*³² in computing periodic orbits. However, in the different contexts, the form of this operator differs as the resulting variational dynamics evolves a spatial or space–time field

representing the specific sought-after invariant solution: In computing equilibria, the variational dynamics evolves a spatial field that geometrically corresponds to moving a point in the state space; in computing periodic orbits, the variational dynamics evolves a space–time field periodic in the temporal direction that corresponds to deforming a loop in the state space, and here the variational dynamics evolves a space–time field satisfying the asymptotic conditions (2) in the temporal direction that corresponds to deforming a curve in the state space that connects two fixed points.

IV. SPECTRAL REPRESENTATION IN TIME

An efficient implementation of the proposed adjoint-based variational method is aided by an accurate spectral representation of a space–time field $\mathbf{q}(\mathbf{x}, s) \in \mathcal{C}_s$ in the s direction such that the asymptotic conditions at $s \rightarrow \pm\infty$ are directly enforced by the chosen expansion. The spectral accuracy significantly reduces the number of time sections, and thereby memory, required for an accurate representation of connecting orbits. We use rational Chebyshev basis functions for the spectral representation in the temporal direction (see Chap. 17 of Ref. 33 for details).

Rational Chebyshev functions, $R_n(s)$, are given by

$$R_n(s) = \cos(n\theta), \quad n \in \mathbb{W}, \quad (16)$$

where $\theta \in (0, \pi)$ and $s \in \mathbb{R}$ are related via

$$s = s_0 + S \cot(\theta) \iff \theta = \cot^{-1} \left(\frac{s - s_0}{S} \right), \quad (17)$$

with $s_0 \in \mathbb{R}$ and $S \in \mathbb{R}^+$ being mapping parameters.

Rational Chebyshev collocation points are obtained by a uniform discretization of θ . Therefore, M interior collocation points are

$$s_j = s_0 + S \cot \left(\frac{j\pi}{M+1} \right), \quad j = 1, 2, \dots, M, \quad (18)$$

with $j = 0$ and $j = M+1$ being reserved for the asymptotic values $s \rightarrow +\infty$ and $s \rightarrow -\infty$, respectively. The uniform discretization of θ results in a non-uniform distribution of grid points in s . Collocation points are denser around s_0 , the center of the distribution, and become sparser further away from the center. The spacing between successive grid points is linearly scaled by S .

A real function $q(s)$ with $s \in \mathbb{R}$ and constant asymptotic values is approximated by the truncated expansion in a rational Chebyshev basis, $q(s) \approx \sum_{k=0}^{M+1} c_k R_k(s)$, where the expansion coefficients are

$$c_k = \frac{2}{(M+1)\tilde{c}_k} \sum_{m=0}^{M+1} \frac{1}{\tilde{c}_m} q(s_m) \cos \left(\frac{mk\pi}{M+1} \right), \quad (19)$$

with grid points s_m defined in equation (18) and

$$\tilde{c}_j = \begin{cases} 2, & \text{if } j = 0 \text{ or } M+1, \\ 1, & \text{otherwise.} \end{cases} \quad (20)$$

Having a grid function $q(s_j)$ with $j = 0, 1, \dots, M+1$ over rational Chebyshev grid points (18), the differentiation matrix D_t is

constructed as

$$D_{t,j,m} = \frac{2}{S(M+1)} \sin^2 \left(\frac{j\pi}{M+1} \right) \sum_{k=0}^{M+1} \frac{k}{\tilde{c}_m \tilde{c}_k} \cos \left(\frac{mk\pi}{M+1} \right) \times \sin \left(\frac{kj\pi}{M+1} \right), \quad j, m = 0, 1, \dots, M+1. \quad (21)$$

The expansion in a rational Chebyshev basis allows us to represent the space–time objects in the unbounded temporal direction, and we can expect spectral accuracy with fast convergence as a function of the expansion's truncation order. Rational Chebyshev functions form a generic basis for the spectral representation of functions over the entire real axis with constant asymptotic values and are, thus, a suitable expansion for connecting orbits for any studied physical system.

V. APPLICATION TO KURAMOTO-SIVASHINSKY EQUATION

As a proof of concept, we apply the introduced method for identifying connecting orbits to the one-dimensional Kuramoto–Sivashinsky equation (KSE).^{34,35} The KSE is a nonlinear partial differential equation, which emerges in various physical contexts such as flame propagation,³⁵ plasma physics,³⁶ or interfacial fluids instability.³⁷ The KSE is also commonly used as a model system for examining new methods developed for chaotic fluid flows and transitional turbulence since it exhibits spatiotemporally chaotic behavior and displays some similar features to the Navier–Stokes equations.

The one-dimensional KSE for a real field $u(x, t)$ on the periodic spatial domain $0 \leq x < L$ is

$$\frac{\partial u}{\partial t} = -u \frac{\partial u}{\partial x} - \frac{\partial^2 u}{\partial x^2} - \nu \frac{\partial^4 u}{\partial x^4}, \quad (22)$$

with constant positive damping parameter ν . The dynamics of the KSE is controlled by the single dimensionless group $\mathbb{L} = L/\sqrt{\nu}$. Here, we fix $\nu = 1$ and consider the domain size L as the control parameter.

For $L < 2\pi$, the trivial equilibrium solution $u(x, t) = \text{const.}$ is linearly stable and is the global attractor of the dynamics. By increasing L , solutions of the KSE undergo a series of bifurcations before the dynamics can exhibit spatiotemporally chaotic behavior for sufficiently large domain sizes. For certain ranges of the control parameter, heteroclinic cycles between equilibria emerge as the most attracting invariant sets. For instance, for $13.03 \lesssim L \lesssim 14.92$, a network of isolated heteroclinic orbits between two symmetry-related equilibrium solutions attracts the nearby trajectories, and the dynamics exhibits regular transitions between the two equilibria.^{38,39} For $18.05 \lesssim L \lesssim 20.89$, we again observe the network of connecting orbits between two symmetry-related equilibria to be attracting. In this range of L , the two equilibria are connected by a one-parameter continuous family of connecting orbits which provides infinitely many heteroclinic cycles and, therefore, transitions take place via irregular bursts.

We demonstrate the application of the proposed method by computing connecting orbits between equilibrium solutions of the KSE for $L = 22$. This domain size is large enough for the KSE

to sustain the spatiotemporally chaotic dynamics. Hence, there is no attracting heteroclinic cycle, and connecting orbits cannot be obtained by time-marching the KSE. However, this domain size is small enough to have low-dimensional unstable manifolds at the equilibria found, over which an exhaustive search for possible connecting orbits is practical. The state space geometry of the KSE for this parameter value has previously been explored in detail by Cvitanović and collaborators.²⁵ They identified several connecting orbits using the shooting method described in Sec. I. Here, at least one connecting orbit between any two equilibrium solutions is computed, or it is confirmed by the exhaustive search in Ref. 25 that no connecting orbit exists between the two equilibria.

A. Formulation of the adjoint-based variational method for the KSE

The KSE (22) has the form of the general dynamical system (1) with $n = d = 1$ and $\Omega = [0, L]$. The residual field, defined in Eq. (5), for the KSE is

$$r = -\frac{\partial u}{\partial s} - u \frac{\partial u}{\partial x} - \frac{\partial^2 u}{\partial x^2} - \frac{\partial^4 u}{\partial x^4}. \quad (23)$$

The dynamical system along whose trajectories the cost function decreases monotonically is derived based on the adjoint operator of the directional derivative of r . The adjoint operator for the KSE system is constructed by a series of integrations by part (see Appendix A for details),

$$\mathcal{L}^\dagger(u; r) = \frac{\partial r}{\partial s} + u \frac{\partial r}{\partial x} - \frac{\partial^2 r}{\partial x^2} - \frac{\partial^4 r}{\partial x^4}. \quad (24)$$

Therefore, the dynamical system in the space of connecting curves, $u(x, s; \tau) \in \mathcal{C}_g$, that minimizes the cost function J^2 is

$$\frac{\partial u}{\partial \tau} = -\mathcal{L}^\dagger(u; r) = -\frac{\partial r}{\partial s} - u \frac{\partial r}{\partial x} + \frac{\partial^2 r}{\partial x^2} + \frac{\partial^4 r}{\partial x^4}. \quad (25)$$

B. Symmetry preservation

The KSE (22) is equivariant under continuous translations in the x -direction

$$\gamma(\alpha)u(x, t) = u(x + \alpha L, t), \quad \alpha \in [0, 1] \quad (26)$$

and under inversions about the origin

$$\sigma u(x, t) = -u(-x, t). \quad (27)$$

The translation operator $\gamma(\alpha)$ and inversion operator σ commute with the residual (23) of the KSE. Consequently, the dynamics in the space of connecting curves, Eq. (25), is equivariant under the action of $\gamma(\alpha)$ and σ . This means that if the integration of Eq. (25) starts from an initial space-time field that is invariant under the action of $\sigma \circ \gamma(\alpha)$, the dynamics preserves the resulting point-inversion symmetry, and, therefore, the computed connecting orbit belongs to the same symmetric subspace of the state space \mathcal{M} .

The KSE (22) preserves the spatial mean value of the evolving field. Consequently, the spatial mean along a connecting orbit is constant and the same as the end point equilibrium solutions. We consider the dynamics of the KSE in the subspace of fields with zero spatial mean. The zero mean value is not enforced during the

evolution of a connecting curve toward a connecting orbit. However, since the two end point equilibria do have zero spatial mean, a converged connecting orbit with $J = 0$ takes zero mean value as well.

C. Numerical implementation

1. Spectral discretization

A connecting curve $u(x, s)$ is discretized in the temporal direction using $M + 2$ time sections (including the end point equilibria) over the rational Chebyshev grid while each time section is represented by N Fourier modes in space,

$$u(x_n, s_m) = \sum_{j=-\frac{N}{2}}^{\frac{N}{2}-1} \hat{u}_j(s_m) \exp\left(j \frac{2\pi x_n}{L} i\right), \quad (28)$$

where $x_n = nL/N$ with indices $0 \leq n < N$ are the uniform grid points in space; s_m with indices $0 \leq m \leq M + 1$ are the non-uniform rational Chebyshev collocation points in time; $\hat{u}_j(s_m)$ is the j th Fourier coefficient of the time section at s_m ; and i is the imaginary unit.

In spectral space, the connecting curve u is represented by an $(M + 2) \times N$ matrix of complex numbers $\hat{u}_{m,j} = \hat{u}_j(s_m)$. The derivative of order $q \in \mathbb{W}$ of this space-time field with respect to x is obtained by the Hadamard product $D_x^{(q)} \odot \hat{u}$, where $D_x^{(q)} = (2\pi ji/L)^q$, and its derivative of order $q \in \mathbb{W}$ with respect to s is obtained by multiplying \hat{u} from the left by D_t^q , where the temporal differentiation matrix D_t is defined in Eq. (21). The residual r and the descent direction G are discretized in the same way with the only difference that their time sections at s_0 and s_{M+1} (corresponding to $s \rightarrow +\infty$ and $s \rightarrow -\infty$, respectively) are identically zero (see Sec. III). The nonlinear terms are calculated in physical space where products are of elementwise Hadamard type. Transforming back and forward between physical and spectral representations of the space-time fields requires one-dimensional forward or backward discrete Fourier transformation of each time section.

2. Initialization

The initial connecting curve is chosen as a convex combination of the equilibrium solutions u_- and u_+ , plus a symmetry breaking term

$$u_0(x, s; a) = \frac{1}{2} \left[(1 + \tanh(s)) u_+(x) + (1 - \tanh(s)) u_-(x) \right] + a \exp(-s^2) v(x), \quad a \in [0, 1], \quad (29)$$

with $x \in [0, L]$ and $s \in \mathbb{R}$. If $u_-(x)$ and $u_+(x)$ both are inversion-symmetric about the same point $x = x_0$, then $a = 0$ results in an initial space-time field for which all time sections are invariant under the same inversion symmetry. Since the proposed variational dynamics preserves the inversion symmetry, we can set $a = 0$ in order to search in the inversion-symmetric subspace of connecting trajectories. In order to break such a symmetry, we add the second line, i.e., set $a \neq 0$, where $v(x)$ is a field which does not have the inversion symmetry shared between $u_-(x)$ and $u_+(x)$.

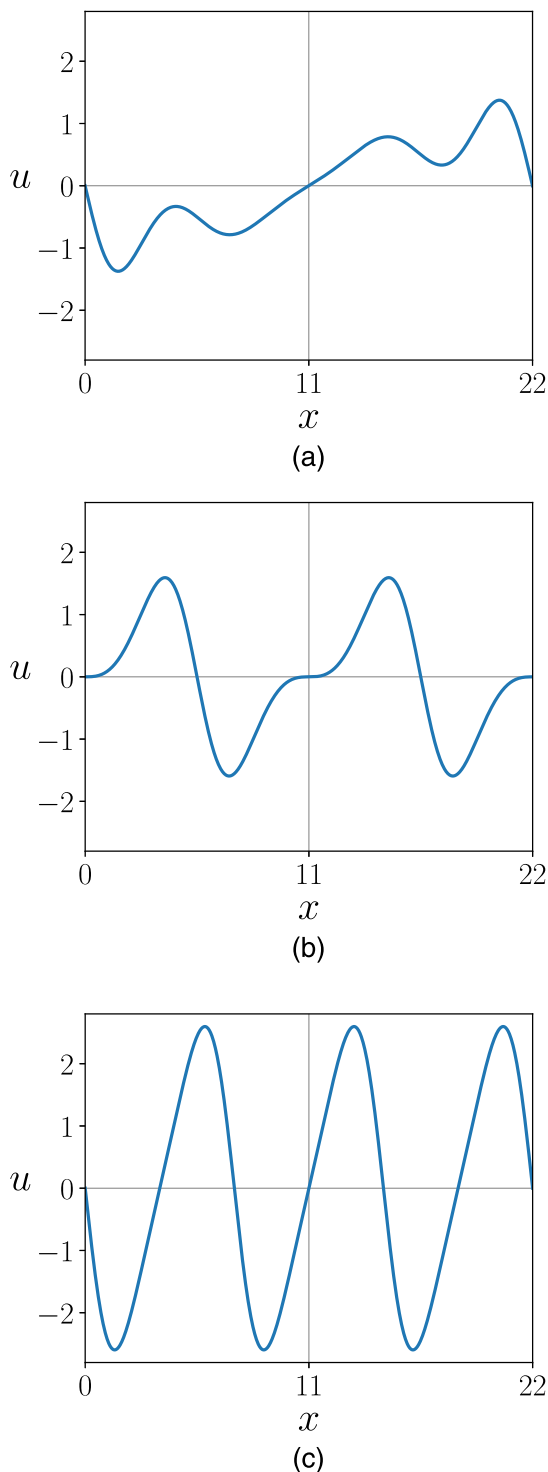


FIG. 2. Nontrivial equilibrium solutions of the KSE for $L = 22$ denoted by (a) E_1 , (b) E_2 , and (c) E_3 . Each of the three solutions is symmetric under inversion about the origin. E_2 and E_3 are also symmetric under discrete shift by $L/2$ and $L/3$, respectively.

TABLE I. Repelling eigenvalues of the equilibria of the KSE for $L = 22$. The rest of the eigenvalues, except one zero eigenvalue for E_1 , E_2 , and E_3 , have a negative real part.

Solution	Unstable eigenvalues
E_0	$\lambda_{1,2} = 0.2198$ $\lambda_{3,4} = 0.1952$ $\lambda_{5,6} = 0.0749$
E_1	$\lambda_{1,2} = 0.1308 \pm 0.3341i$ $\lambda_{3,4} = 0.0824 \pm 0.3402i$
E_2	$\lambda_{1,2} = 0.1390 \pm 0.2384i$
E_3	$\lambda_{1,2} = 0.0933$

3. Time stepping

The defined dynamical system $\partial u / \partial \tau = G$ is globally contractive and we are only concerned about the asymptotic state $u = u_0 + \int_0^\infty G d\tau$. Consequently, we select the numerical integration scheme based on simplicity and stability rather than accuracy. We use semi-implicit forward Euler time-stepping scheme, which has first-order accuracy in τ and treats the linear terms of G in u implicitly and the nonlinear terms explicitly. The code was developed in C++ with OpenMP parallelization of local calculations.

D. Results and discussion

In the subspace of fields with zero spatial mean, the KSE with $L = 22$ has four known equilibrium solutions including the trivial solution $u = 0$. Hereafter, we denote the trivial equilibrium solution by E_0 , and the nontrivial ones by E_1 , E_2 , and E_3 as shown in Fig. 2. We compute these equilibrium solutions following the adjoint-based variational method of Farazmand.³¹ E_1 , E_2 , and E_3 are invariant under inversion about the origin, σ . E_2 and E_3 are also symmetric under discrete shifts $\gamma(1/2)$ and $\gamma(1/3)$, respectively.

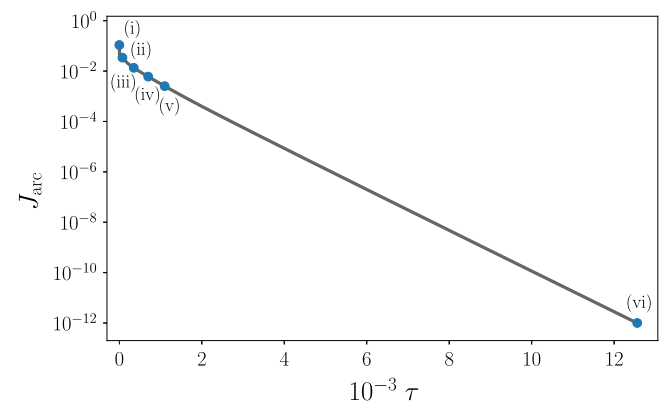


FIG. 3. Monotonic decrease of the arc length cost function J_{arc} against the fictitious time τ as the dynamics in the space of connecting curves evolves an initial connecting curve toward a connecting orbit for which $J = 0$. A three-dimensional projection of the state space corresponding to the marked times (i) to (vi) is shown in Fig. 4.

Therefore, in addition to the inversion about $x = 0$ and $L/2$, E_2 is symmetric under inversion about $x = L/4$ and $3L/4$, and E_3 is symmetric under inversion about $x = L/6$, $L/3$, $2L/3$, and $5L/6$ as well. The repelling eigenvalues of all four equilibrium solutions are listed in Table I, and their associated eigenvectors are shown in Figs. 15–18 in Appendix B.

Connecting orbits are converged by integrating Eq. (25) until a fixed point in the vector field of G , corresponding to a minimum J , is achieved. Connecting orbits correspond to the global minima of J ,

for which $J = 0$. In order to monitor the convergence, we define the arc length weighted cost function

$$J_{\text{arc}} = \frac{\int_{-\infty}^{+\infty} |\mathbf{r}| \left| \frac{\partial \mathbf{u}}{\partial s} \right| ds}{\int_{-\infty}^{+\infty} \left| \frac{\partial \mathbf{u}}{\partial s} \right| ds}, \quad (30)$$

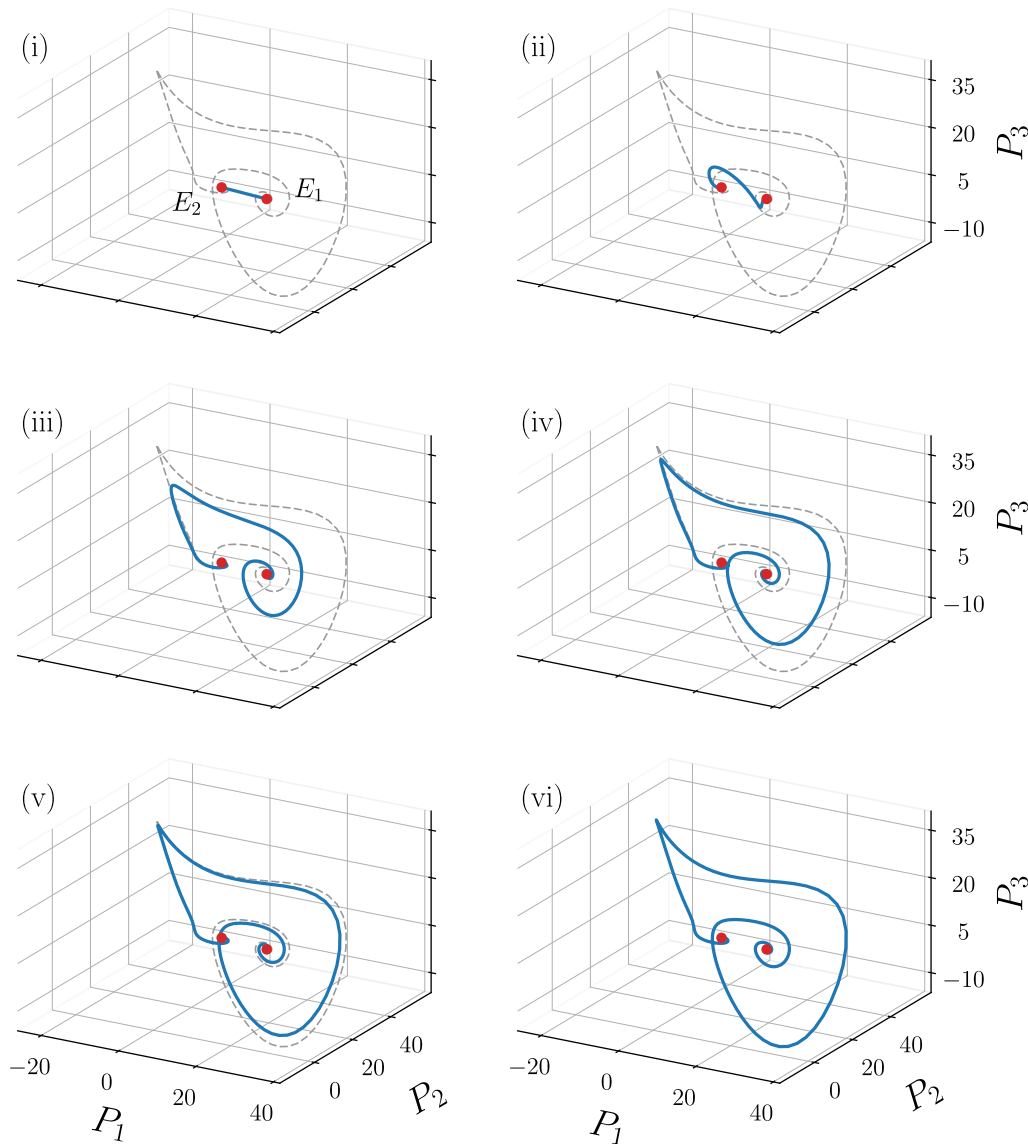


FIG. 4. Continuous deformation of a connecting curve by the dynamics constructed in the space of connecting curves toward a heteroclinic connection from the fixed point E_1 to E_2 . The solid blue line is the evolving connecting curve at the times marked on Fig. 3, and the dashed line is the converged heteroclinic connection. The state space is projected on $P_k(s) = \Im\{\hat{u}_k(s)\}$, $k = 1, 2, 3$.

with $|\cdot|$ being

$$|\mathbf{q}| = \sqrt{\int_{\Omega} \mathbf{q} \cdot \mathbf{q} \, d\mathbf{x}}, \quad \mathbf{q} \in \mathcal{C}_s. \quad (31)$$

Obviously, $J_{\text{arc}} = 0$ if and only if $J = 0$. However, the numerical evaluation of J_{arc} is not subject to the error accumulation associated with the numerical evaluation of the improper integral (4) that defines J . Moreover, since the trivial solution to the definition of a homoclinic connection has zero arc length, J_{arc} is undefined when the trivial solution is achieved, while $J = 0$ for either trivial or nontrivial solutions. We consider the algorithm converged when $J_{\text{arc}} < 10^{-12}$.

Due to the continuous translational symmetry of the KSE, E_i with $i = 1, 2, 3$ represent their so-called group orbits of all symmetry-related states, i.e., $\gamma(\alpha)E_i$ where $\alpha \in [0, 1]$. Every connecting orbit, therefore, has infinite dynamically equivalent copies corresponding to similar translations of the origin and the destination equilibrium solutions. We search for connecting orbits of a certain relative phase between the two end points by fixing the origin equilibrium and shifting the destination equilibrium solution when constructing the initial connecting curve using Eq. (29). In the following, we first demonstrate the application of the introduced method by computing a connecting orbit from E_1 to E_2 . We then present converged connecting orbits between other equilibrium solutions and compare them to the same orbits obtained from other methods reported in the literature if applicable.

The search for a heteroclinic connection from E_1 to E_2 is initialized by a connecting curve constructed using Eq. (29) in the inversion-symmetric subspace of \mathcal{M} ($a = 0$). We discretize the space-time domain by $N = 64$ Fourier modes in space and $M = 550$ rational Chebyshev grid points in time. The scaling of the temporal discretization is set to $S = 55$ and the center of the distribution to $s_0 = 0$. For this system, the integration scheme described in Sec. V C is stable for $\Delta\tau = 0.01$.

After a sharp initial decrease, the arc length cost function decays exponentially with the fictitious time, as shown in Fig. 3, and reaches the convergence criterion, $J_{\text{arc}} = 10^{-12}$, at $\tau \approx 1.25 \times 10^4$. In the vector field induced by G , heteroclinic connections are attracting fixed points. The exponential decay of the cost function suggests that when the evolving connecting curve gets close enough to the connecting orbit, the dynamics is dominated by the leading, i.e., the slowest, eigendirection of the linearized dynamics in the vicinity of the fixed point of $\partial\mathbf{u}/\partial\tau = G$.

Figure 4 shows six snapshots of the continuous deformation of the connecting curve from E_1 to E_2 governed by the dynamics in the space of connecting curves (25) toward a heteroclinic connection. A substantial deformation toward the final shape of the connecting orbit takes place at the beginning of the evolution. The major remaining part of the integration time is spent on the slight remaining deviation from the final orbit. The space-time field corresponding to the initial connecting curve [snapshot (i) in Fig. 4] and the converged connecting orbit [snapshot (vi) in Fig. 4] are displayed in panels (a) and (b) of Fig. 5, respectively.

The spatial resolution is chosen by monitoring the energy spectrum of spatial Fourier modes in a direct numerical simulation of the KSE for $L = 22$. The spatial resolution $N = 64$ ensures at least

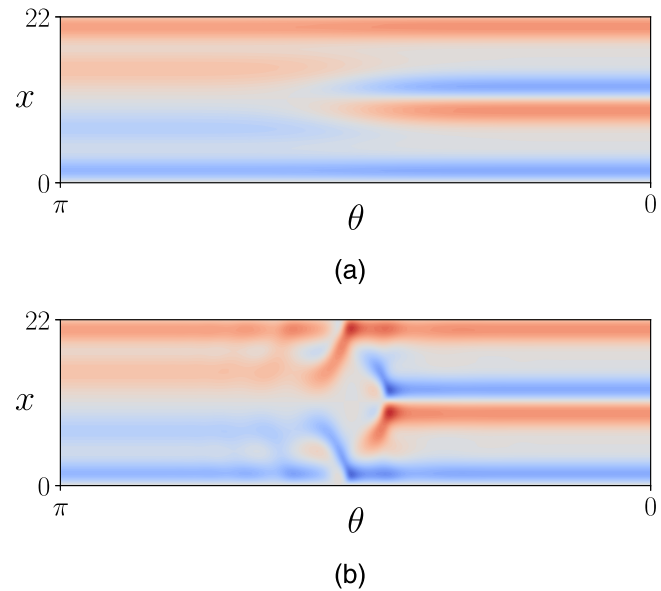


FIG. 5. The space-time contour of the initial connecting curve and the converged connecting orbit from the equilibrium solution E_1 to E_2 . The initial connecting curve is symmetric under inversion about the origin. Since the dynamics in the space of connecting curves preserves the center symmetry, the converged connecting orbit belongs to center-symmetric subspace as well. The temporal dimension is mapped on the uniformly discretized finite interval $[\pi, 0]$, where $\theta = \pi$ and $\theta = 0$ correspond to $s \rightarrow -\infty$ and $s \rightarrow +\infty$, respectively [see Eq. (18)]. (a) The initial connecting curve at $\tau = 0$. See marker (i) on Fig. 3 and panel (i) of Fig. 4. (b) The converged connecting orbit at $\tau = 1.25 \times 10^4$. See marker (vi) on Fig. 3 and panel (vi) of Fig. 4.

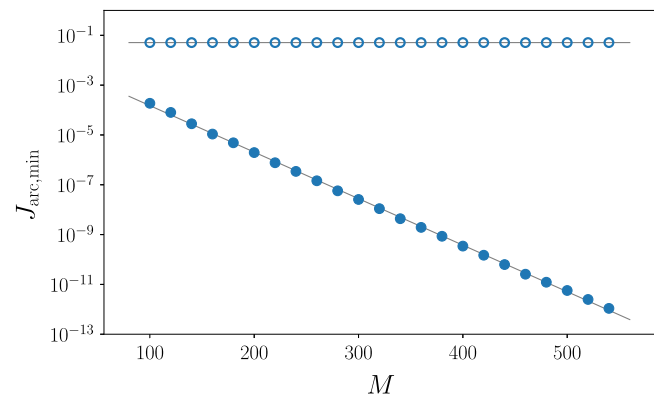


FIG. 6. Variation of the asymptotic value of the arc length cost function J_{arc} by refining the temporal resolution M . Filled circles: Exponential decrease of $J_{\text{arc,min}}$ to zero in successfully converging to a connecting orbit from E_1 to E_2 . Open circles: The cost function gets stuck in a local minimum in the failed search for a connecting orbit from E_2 to $\gamma(1/4)E_2$ in an over-constrained subspace.

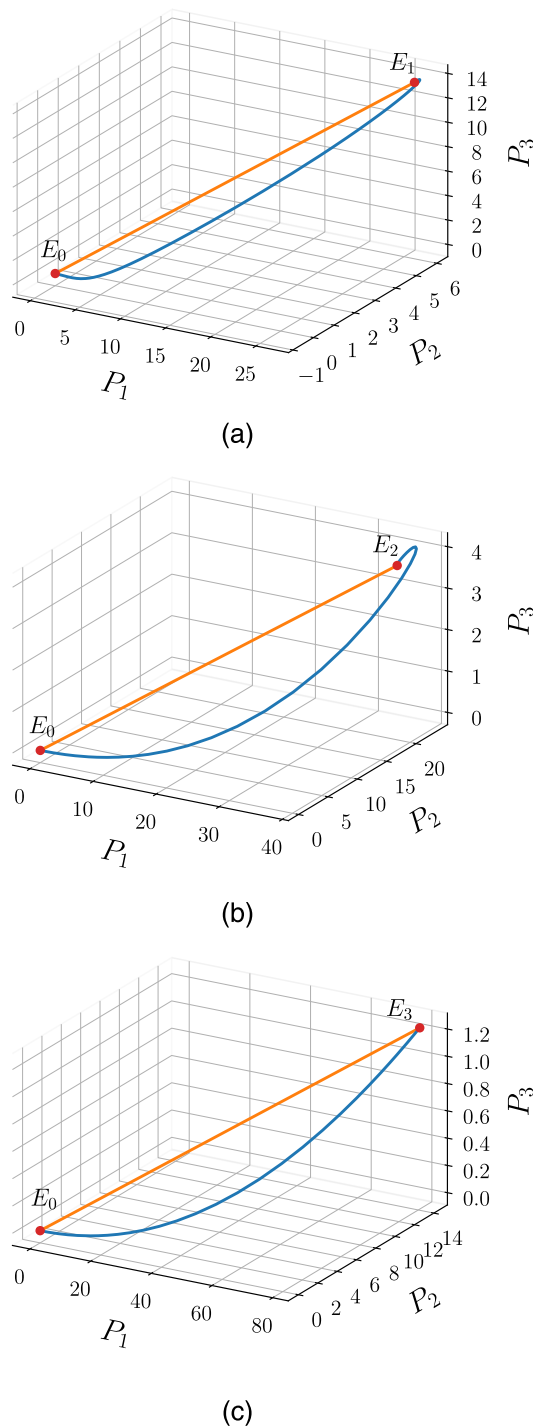


FIG. 7. Connecting orbits from E_0 to (a) E_1 , (b) E_2 , and (c) E_3 in the center-symmetric subspace. The orange line shows the initial connecting curve, and the blue line shows the converged connecting orbit. The state space is projected on $P_k(s) = \Re\{\hat{u}_{bk}(s)\}$, $k = 1, 2, 3$ with $b = 1$ in (a), $b = 2$ in (b), and $b = 3$ in (c).

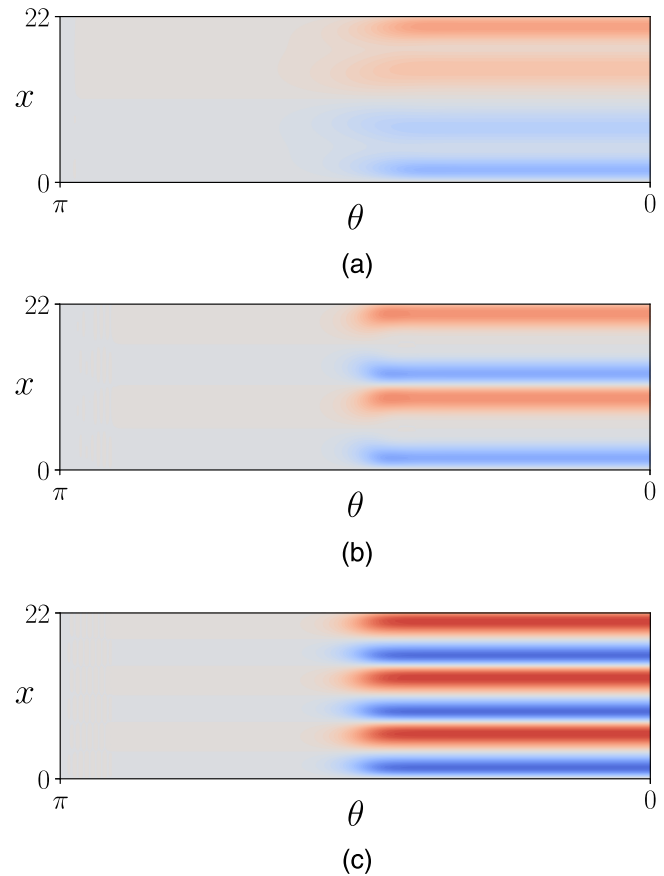


FIG. 8. The space-time contour of the converged connecting orbits from E_0 to (a) E_1 , (b) E_2 , and (c) E_3 in the center-symmetric subspace.

six orders of magnitude drop in the modulus of spatial Fourier coefficients at all times. The converged connecting orbit from E_1 to E_2 , as an equilibrium solution to Eq. (25), is structurally stable for a wide range of temporal resolutions M . However, the accuracy of the spectral representation in time, and therefore the minimum achieved value of the cost function, $J_{\text{arc},\min} := \lim_{\tau \rightarrow \infty} J_{\text{arc}}(\tau)$, varies with M . Figure 6 show the spectral convergence of $J_{\text{arc},\min}$ with M . Notice that $J_{\text{arc},\min}$ can be considerably higher than the convergence criterion when M is not large enough. If a local minimum of the cost function is reached, in contrast, $J_{\text{arc},\min}$ does not improve as the temporal resolution is increased. As an example of a failing search, we try to converge a connecting orbit between E_2 and $\gamma(1/4)E_2$ from an initial connecting curve constructed using Eq. (29) with $a = 0$ (see Sec. V C 3 why such connection cannot exist). The integration from this initial connecting curve does not reach a global minimum but approaches a local minimum with $J_{\text{arc},\min} = 5.1 \times 10^{-2}$. As shown on Fig. 6, the minimum value does not decrease as the temporal discretization is refined, confirming that a converged local minimum has been identified and no connecting orbit was found.

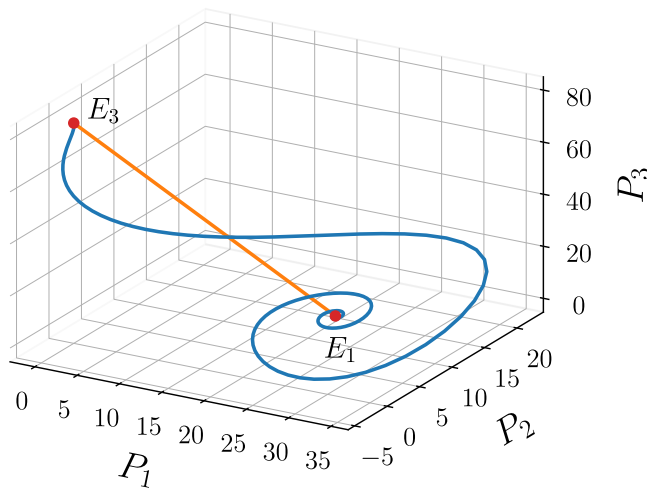


FIG. 9. Connecting orbit from E_1 to E_3 in the center-symmetric subspace. The orange line shows the initial connecting curve, and the blue line shows the converged connecting orbit. The state space is projected on $P_k(s) = \Re\{\hat{u}_k(s)\}$, $k = 1, 2, 3$.

1. Connecting orbits originating from E_0 : Six-dimensional unstable manifold

We converge a heteroclinic connection from E_0 to E_1 , E_2 and E_3 from an initial connecting curve constructed using Eq. (29) with $a = 0$. A three-dimensional state space projection and the space-time contour of heteroclinic connections from E_0 to the other three equilibrium solutions are exhibited in Figs. 7 and 8, respectively. The algorithm settings are presented in Appendix C.

The unstable manifold of E_0 is six-dimensional. Each of the repeated unstable eigenvalues of E_0 , Table I, is associated with one eigenvector symmetric under reflection across $x = 0$ and another one symmetric under inversion about the origin (see Fig. 15). An exhaustive search in the unstable tangent space at E_0 is not practical even in the inversion-symmetric subspace of the KSE where the reflection-symmetric eigenvectors do not exist, and the unstable manifold is three-dimensional. Dong and Lan²⁸ have computed a heteroclinic connection from E_0 to E_1 using their variational method, which employs finite differences for calculating tangent velocity vectors. They have used 6000 sections to discretize this

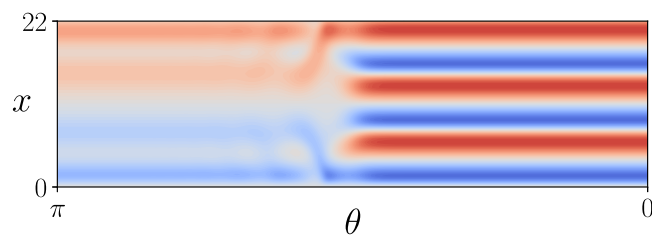
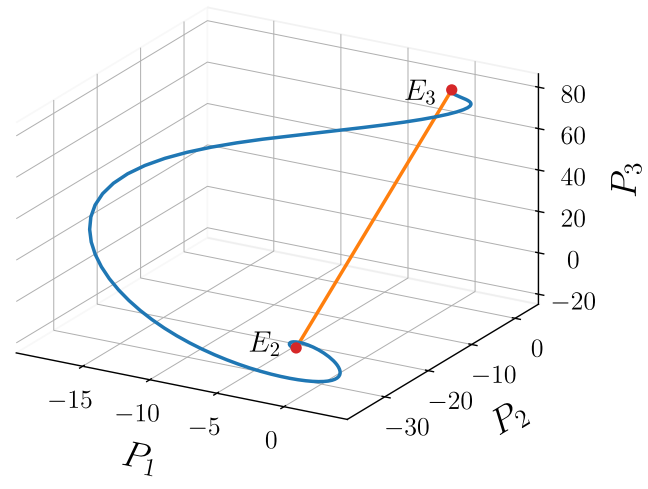
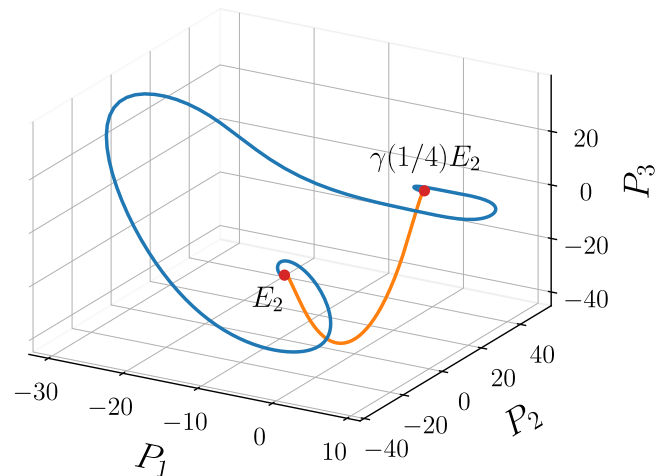


FIG. 10. The space-time contour of the converged connecting orbit from E_1 to E_3 in the center-symmetric subspace.



(a)



(b)

FIG. 11. Connecting orbits from E_2 to (a) E_3 and (b) $\gamma(1/4)E_2$ in the center-symmetric subspace. The orange line shows the initial connecting curve, and the blue line shows the converged connecting orbit. The state space is projected on $P_k(s) = \Re\{\hat{u}_k(s)\}$, $k = 1, 2, 3$.

connecting orbit in time and obtain residuals of order $\mathcal{O}(10^{-6})$. To achieve this value of J_{arc} (and similarly, the supremum norm of the residual r), $M = 25$ interior time sections suffice for the proposed variational method.

2. Connecting orbits originating from E_1 : Four-dimensional unstable manifold

We demonstrated the details of converging a heteroclinic connection from E_1 to E_2 at the beginning of this section (see Figs. 3–6).

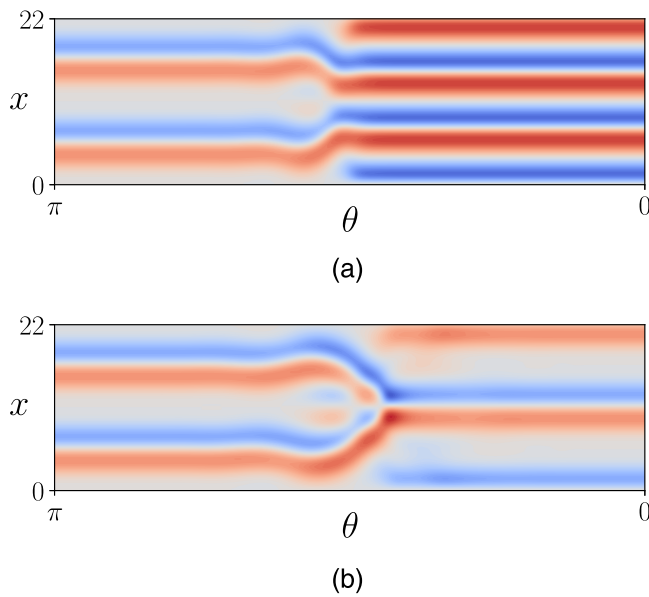


FIG. 12. The space-time contour of the converged connecting orbits from E_2 to (a) E_3 and (b) $\gamma(1/4)E_2$ in the center-symmetric subspace.

We also converge a heteroclinic connection from E_1 to E_3 from an initial connecting curve constructed using Eq. (29) with $a = 0$. Figures 9 and 10 show a three-dimensional state space projection and the space-time contour plot of the converged heteroclinic connection from E_1 to E_3 , respectively. The algorithm settings are presented in Appendix C.

The unstable manifold of E_1 is four-dimensional. One pair of complex conjugate unstable eigenvalues of E_1 , Table I, is associated with eigenvectors invariant under reflection across $x = 0$, while the other pair is associated with eigenvectors invariant under inversion about the origin (see Fig. 16). An exhaustive search in the four-dimensional unstable tangent space at E_1 is not practical. Cvitanović *et al.*²⁵ perform an exhaustive search in the two-dimensional plane spanned by the reflection-symmetric eigenvectors at E_1 and show that all trajectories starting from that plane are chaotic and do not reach any of the equilibrium solutions. They perform another exhaustive search in the two-dimensional plane spanned by the inversion-symmetric eigenvectors and show that trajectories starting from that plane form a one-parameter family of heteroclinic connections from E_1 to E_2 , except one bordering orbit that converges to E_3 .

3. Connecting orbits originating from E_2 : Two-dimensional unstable manifold

We converge two heteroclinic connections from E_2 to E_3 and $\gamma(1/4)E_2$. The initial conditions are constructed using Eq. (29) by setting $a = 0$ for the connecting orbit between E_2 and E_3 and setting $a = -1$ and $v = \Re\{v_{1,2}\}$ for the connecting orbit between E_2 and $\gamma(1/4)E_2$, where $\Re\{v_{1,2}\}$ is the real part of the complex conjugate unstable eigenvectors at E_2 (see Fig. 17). In the latter, adding

the symmetry breaking term ($a \neq 0$) is necessary because E_2 and $\gamma(1/4)E_2$ are both symmetric under inversion about $x = kL/4$ with $k = 0, 1, 2, 3$, thus, an initial connecting curve constructed by setting $a = 0$ is symmetric under inversion about all these points. The dynamics (25) preserves all the four inversion symmetries while no connecting orbit can exist in such subspace of \mathcal{M} because the unstable eigenvectors of E_2 are symmetric only about $x = 0$ and $L/2$, meaning that as soon as a trajectory of the KSE leaves E_2 , the

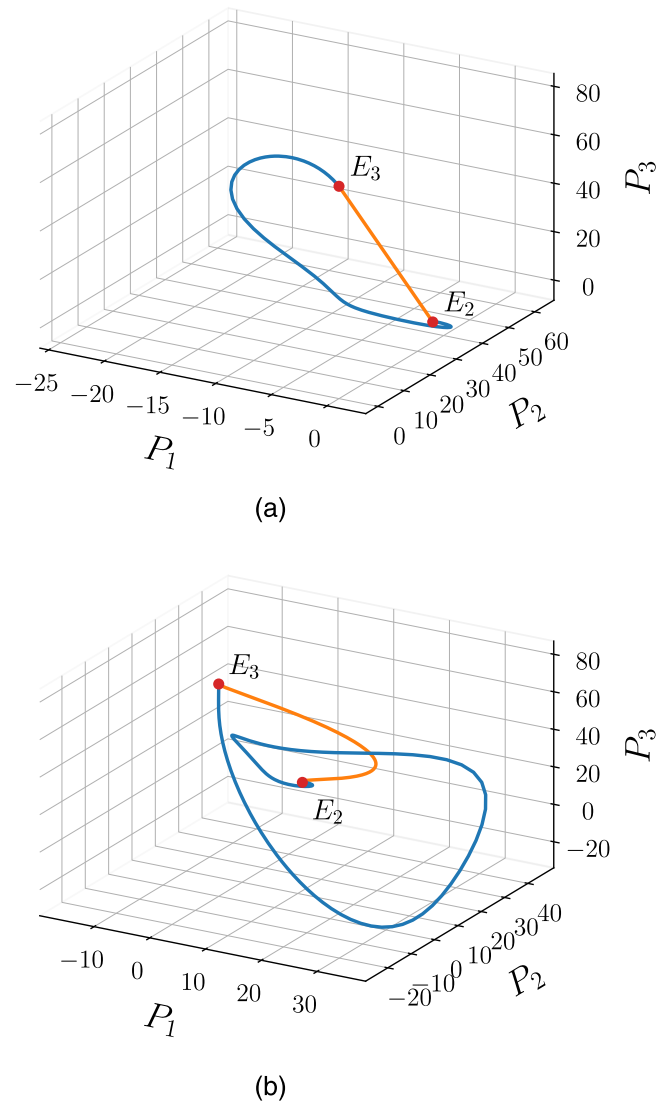


FIG. 13. Two connecting orbits from E_3 to E_2 in the center-symmetric subspace. The orange line shows the initial connecting curve, and the blue line shows the converged connecting orbit. The state space is projected on $P_k(s) = \Re\{\hat{u}_k(s)\}$, $k = 1, 2, 3$. (a) Orbit 1: The initial connecting curve is constructed via Eq. (29) by setting $a = 0$. (b) Orbit 2: The initial connecting curve is constructed via Eq. (29) by setting $a = -1$ and $v = \sin(x)$.

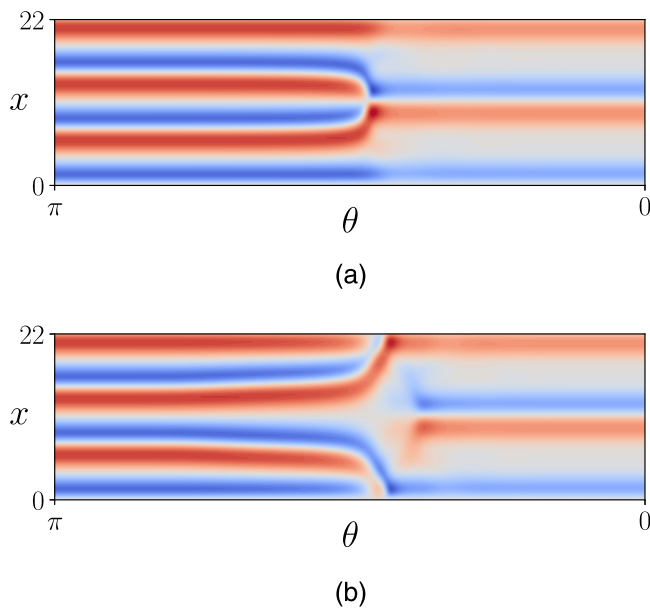


FIG. 14. The space–time contour of the two converged connecting orbits from E_3 to E_2 in the center-symmetric subspace: (a) Orbit 1 and (b) orbit 2. See Fig. 13.

inversion symmetries about $x = L/4$ and $3L/4$ are broken. Consequently, as shown in Fig. 6, $a = 0$ results in getting stuck in a local minimum of the cost function as the dynamics (25) is integrated. A three-dimensional state space projection and the space–time contour plot of the connecting orbits from E_2 to E_3 and $\gamma(1/4)E_2$ are shown in Figs. 11 and 12, respectively. The algorithm settings are presented in Appendix C.

By an exhaustive search in the two-dimensional unstable tangent space at E_2 , Cvitanović *et al.*²⁵ show that the unstable manifold of E_2 is a one-parameter family of connecting orbits that converge to $\gamma(1/4)E_2$, except one orbit that connects E_2 to E_3 .

4. Connecting orbits originating from E_3 : Two-dimensional unstable manifold

We converge two heteroclinic connections from E_3 to E_2 . The initial conditions are constructed using Eq. (29) by setting $a = 0$ in one and $a = -1$ and $v = \sin(x)$ in the other. A three-dimensional state space projection and the space–time contour of these connecting orbits are shown in Figs. 13 and 14, respectively. The algorithm settings are presented in Appendix C.

The unstable manifold of E_3 is two-dimensional. The repeated positive eigenvalue of E_3 , Table I, is associated with one eigenvector symmetric under reflection across $x = 0$, and another eigenvector symmetric under inversion about the origin (see Fig. 18). Cvitanović *et al.*²⁵ conduct an exhaustive search in the two-dimensional unstable tangent space at E_3 and identify two heteroclinic connections from E_3 to E_2 corresponding to the perturbation of E_3 along the inversion-symmetric eigenvector and its opposite direction. Fixing E_3 and shifting E_2 in space by $L/3$ and $2L/3$ puts the translated copy

of E_2 in the same relative phase to E_3 as the original configuration. Therefore, the exhaustive search identifies two other pairs of heteroclinic connections from E_3 to the group orbit of E_2 , which are copies of the first pair of connecting orbits shifted by $L/3$ and $2L/3$ in the x -direction.

VI. SUMMARY AND CONCLUDING REMARKS

Connecting orbits are of significant importance for studying spatiotemporally chaotic dynamical systems in terms of their invariant state space structures. We introduce a variational method for computing connecting orbits between two equilibrium solutions by searching in the space of all smooth curves in the state space that connect the two equilibria. In this method, the deviation of a connecting curve from an integral curve of the vector field is penalized by a non-negative cost function. A dynamical system in the space of connecting curves is set up such that along its trajectories the cost function is guaranteed to decrease monotonically. All trajectories of this dynamical system eventually converge to an equilibrium, which corresponds to a minimum of the cost function. Global minima of the cost function, taking zero value, correspond to the connecting orbits of the original dynamics. This method is not limited by the dimensionality of the unstable manifold at the origin equilibrium solution, does not suffer from exponential separation of trajectories, and does not require any domain truncation. The introduced method is Jacobian-free, and its memory requirement scales linearly with the number of degrees of freedom, which allows this method to be applied to high-dimensional dynamical systems including three-dimensional fluid dynamics problems.

As a proof of concept, we apply the introduced variational method to the one-dimensional KSE and compute several connecting orbits between known equilibrium solutions of the system with domain size $L = 22$. The set of converged solutions contains at least one connecting orbit between any two equilibrium solutions unless it is known from an exhaustive search in the unstable manifold of the origin equilibrium solution that they are not connected. The stability analysis of the adjoint-descent dynamics (25) can determine if the identified solution is an isolated connecting orbit or belongs to a one-parameter continuous family of orbits. In the former case, all eigenvalues are negative except only one zero associated with continuous translations in the temporal direction s . In the latter, the stability matrix has an additional zero associated with variation within the continuous family of connecting orbits. In that case, the connecting surface can be computed by tracing the neutral eigendirection associated with the second zero eigenvalue.

After demonstrating the feasibility of the introduced method for computing connecting orbits between equilibrium solutions of the one-dimensional KSE, we are extending the present work in two directions: One is applying this method to the three-dimensional wall-bounded fluid flows governed by the Navier–Stokes equations (NSEs). The challenge in applying this method to the wall-bounded NSEs lies not only in dealing with a dynamical system of considerably larger size but also in handling the incompressibility constraint and the pressure field. Pressure is not governed by an explicit evolution equation but by the so-called pressure Poisson equation to adapt itself to the velocity such that the velocity field remains

divergence-free. An accurate computation of the pressure field associated with an instantaneous divergence-free velocity field in a wall-bounded domain is not a trivial task,⁴⁰ let alone the derivation of the adjoint operator in the presence of this nonlocal, nonlinear operator. The second direction is developing methods following a similar idea for computing connecting orbits between invariant solutions of other types, including between two periodic orbits and eventually between invariant tori. This requires to reformulate the variational dynamics within modified search spaces appropriate for the different asymptotic boundary conditions in the temporal direction. Together with improved methods for computing other invariant solutions,^{32,41,42} the proposed methodology for computing connecting orbits represents a step toward a more complete description of the state-space structures supporting spatiotemporally chaotic dynamics. Eventually, the identification of connecting orbits mediating transitions between invariant solutions may allow for efficient forecasting of chaos even in high-dimensional systems including fluid turbulence.

ACKNOWLEDGMENTS

This research has been supported by the European Research Council (ERC) under the European Union's Horizon 2020 research and innovation programme (Grant Agreement No. 865677). The authors would like to thank Sajjad Azimi and Jeremy P. Parker for their helpful discussions.

AUTHOR DECLARATIONS

Conflict of Interest

The authors have no conflicts to disclose.

Author Contributions

Omid Ashtari: Conceptualization (equal); Investigation (equal); Methodology (equal); Software (lead); Writing – original draft (equal); Writing – review & editing (equal). **Tobias M. Schneider:** Conceptualization (equal); Funding acquisition (lead); Investigation (equal); Methodology (equal); Supervision (lead); Writing – original draft (equal); Writing – review & editing (equal).

DATA AVAILABILITY

The data that support the findings of this study are available from the corresponding author upon reasonable request.

APPENDIX A: DERIVATION OF THE ADJOINT OPERATOR FOR THE KSE

The directional derivative of the residual of the KSE, defined in Eq. (23), along G is obtained by definition (12) as

$$\mathcal{L}(u; G) = -\frac{\partial G}{\partial s} - \frac{\partial(uG)}{\partial x} - \frac{\partial^2 G}{\partial x^2} - \frac{\partial^4 G}{\partial x^4}. \quad (\text{A1})$$

In order to find the adjoint operator, we expand the inner product of $\mathcal{L}(u; G)$ and r as

$$\begin{aligned} \langle \mathcal{L}(u; G), r \rangle &= \int_{-\infty}^{+\infty} \int_0^L \left(-\frac{\partial G}{\partial s} - \frac{\partial(uG)}{\partial x} - \frac{\partial^2 G}{\partial x^2} - \frac{\partial^4 G}{\partial x^4} \right) r \, dx \, ds \\ &= - \int_0^L \left\{ \int_{-\infty}^{+\infty} \frac{\partial G}{\partial s} r \, ds \right\} dx - \int_{-\infty}^{+\infty} \left\{ \int_0^L \left(\frac{\partial(uG)}{\partial x} \right. \right. \\ &\quad \left. \left. + \frac{\partial^2 G}{\partial x^2} + \frac{\partial^4 G}{\partial x^4} \right) r \, dx \right\} ds. \end{aligned} \quad (\text{A2})$$

Integrating by parts, we can write the first and the second integral as follows:

$$\int_0^L \left\{ \int_{-\infty}^{+\infty} \frac{\partial G}{\partial s} r \, ds \right\} dx = \int_0^L \left\{ \lim_{T \rightarrow \infty} [Gr]_{s=-T}^{s=T} - \int_{-\infty}^{+\infty} G \frac{\partial r}{\partial s} \, ds \right\} dx,$$

$$\begin{aligned} &\int_{-\infty}^{+\infty} \left\{ \int_0^L \left(\frac{\partial(uG)}{\partial x} + \frac{\partial^2 G}{\partial x^2} + \frac{\partial^4 G}{\partial x^4} \right) r \, dx \right\} ds \\ &= \int_{-\infty}^{+\infty} \left\{ [uGr]_{x=0}^{x=L} - \int_0^L uG \frac{\partial r}{\partial x} \, dx + \left[\frac{\partial G}{\partial x} r - G \frac{\partial r}{\partial x} \right]_{x=0}^{x=L} \right. \\ &\quad \left. + \int_0^L G \frac{\partial^2 r}{\partial x^2} \, dx + \left[\frac{\partial^3 G}{\partial x^3} r - \frac{\partial^2 G}{\partial x^2} \frac{\partial r}{\partial x} \right. \right. \\ &\quad \left. \left. + \frac{\partial G}{\partial x} \frac{\partial^2 r}{\partial x^2} - G \frac{\partial^3 r}{\partial x^3} \right]_{x=0}^{x=L} + \int_0^L G \frac{\partial^4 r}{\partial x^4} \, dx \right\} ds. \end{aligned}$$

In the limit $T \rightarrow \infty$, the boundary term $[Gr]_{s=-T}^{s=T}$ vanishes since both G and r are asymptotically zero. All boundary terms, $[\cdot]_{x=0}^{x=L}$, vanish too due to periodicity of u , r , and G in x . Therefore, Eq. (A2) becomes

$$\langle \mathcal{L}(u; G), r \rangle = \int_{-\infty}^{+\infty} \int_0^L \left(\frac{\partial r}{\partial s} + u \frac{\partial r}{\partial x} - \frac{\partial^2 r}{\partial x^2} - \frac{\partial^4 r}{\partial x^4} \right) G \, dx \, ds. \quad (\text{A3})$$

From the definition of the adjoint operator (14), this inner product equals

$$\langle \mathcal{L}^\dagger(u; r), G \rangle = \int_{-\infty}^{+\infty} \int_0^L \mathcal{L}^\dagger G \, dx \, ds. \quad (\text{A4})$$

Comparing Eqs. (A3) and (A4), $\mathcal{L}^\dagger(u; r)$ is given by

$$\mathcal{L}^\dagger(u; r) = \frac{\partial r}{\partial s} + u \frac{\partial r}{\partial x} - \frac{\partial^2 r}{\partial x^2} - \frac{\partial^4 r}{\partial x^4}. \quad (\text{A5})$$

APPENDIX B: UNSTABLE EIGENVECTORS OF THE EQUILIBRIA OF THE KSE

The KSE with $L = 22$ has four known equilibrium solutions including the trivial solution $E_0 = 0$, and three nontrivial solutions E_1 , E_2 , and E_3 as shown in Fig. 2. The repelling eigenvalues of these equilibrium solutions are listed in Table I. The corresponding eigenvectors of E_0 , E_1 , E_2 , and E_3 are shown in Figs. 15–18, respectively.

APPENDIX C: PARAMETERS USED IN COMPUTING CONNECTING ORBITS OF THE KSE

In all calculations presented in Sec. V, we have used $N = 64$ Fourier modes in space, have set the center of the temporal distribution at the origin $s_0 = 0$, and have used time step size $\Delta\tau = 0.01$. The temporal resolution M and the scaling S are listed in Table II. The temporal resolution is set high enough so that the convergence criterion $J_{\text{arc,min}} < 10^{-12}$ is achieved (see Sec. V D).

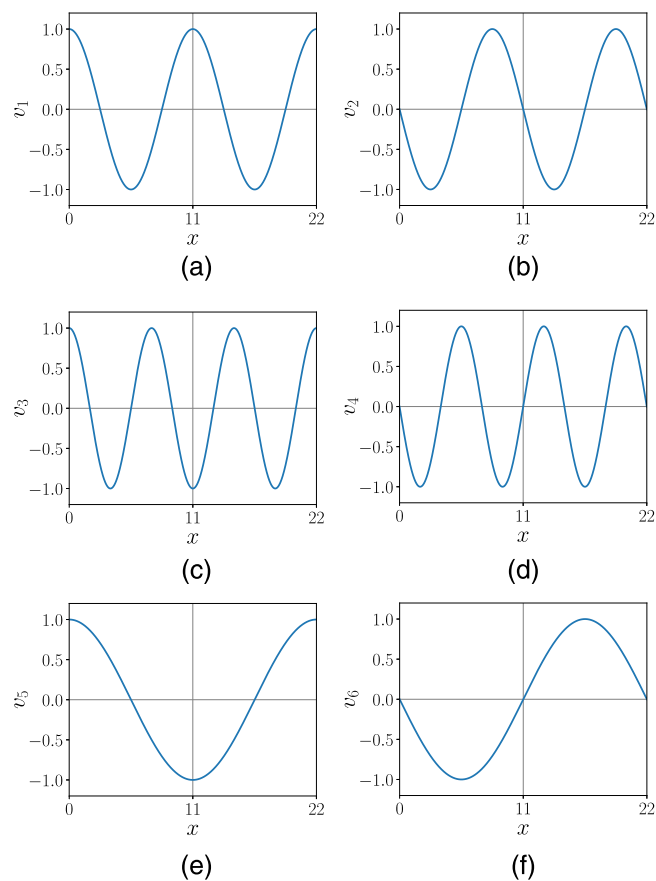


FIG. 15. Unstable eigenvectors v_i of the trivial equilibrium solution E_0 . The associated eigenvalues are $\lambda_{1,2} = 0.2198$ in (a) and (b), $\lambda_{3,4} = 0.1952$ in (c) and (d), and $\lambda_{5,6} = 0.0749$ in (e) and (f).

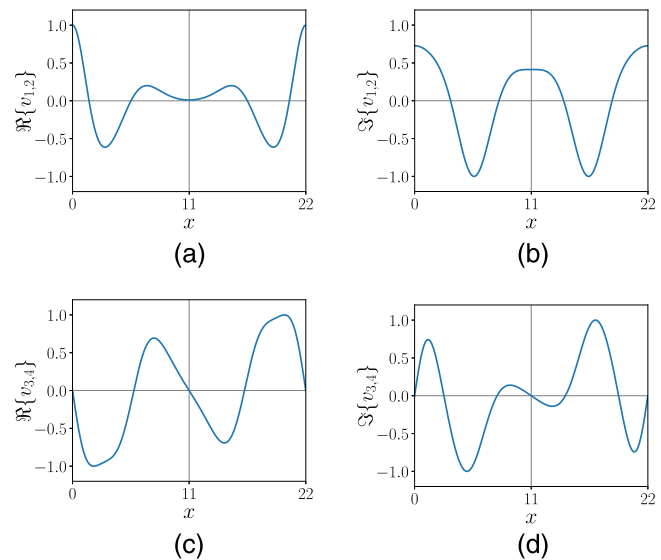


FIG. 16. Unstable eigenvectors v_i of the equilibrium solution E_1 . The associated eigenvalues are $\lambda_{1,2} = 0.1308 \pm 0.3341i$ in (a) and (b), and $\lambda_{3,4} = 0.0824 \pm 0.3402i$ in (c) and (d).

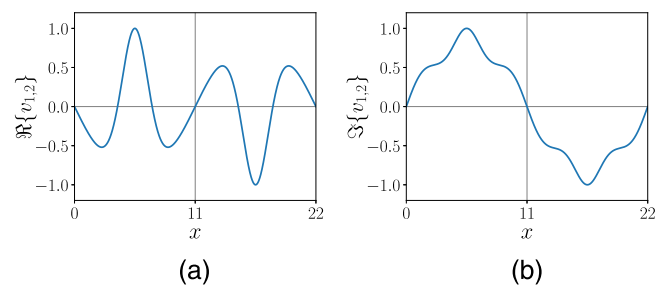


FIG. 17. Unstable eigenvectors v_i of the equilibrium solution E_2 . The associated eigenvalues are $\lambda_{1,2} = 0.1390 \pm 0.2384i$.

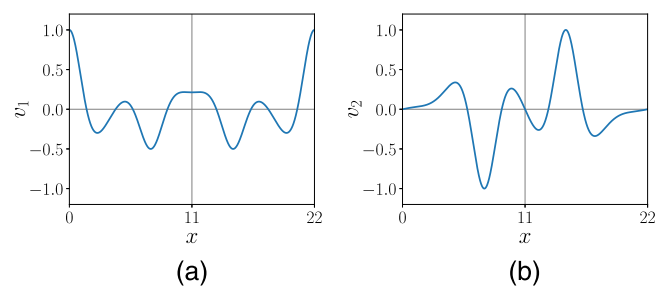


FIG. 18. Unstable eigenvectors v_i of the equilibrium solution E_3 . The associated eigenvalues are $\lambda_{1,2} = 0.0933$.

TABLE II. Parameters used for numerically integrating the dynamics in the space of connecting curves between different equilibrium solutions of the KSE for $L = 22$ to compute connecting orbits.

Row	From	To	M	S	Figures
1	E_0	E_1	80	40	7(a) and 8(a)
2		E_2	130	35	7(b) and 8(b)
3		E_3	120	40	7(c) and 8(c)
4	E_1	E_2	550	55	4 and 5
5		E_3	500	60	9 and 10
6	E_2	$\tau(1/4)E_2$	400	35	11(a) and 12(a)
7		E_3	450	50	11(b) and 12(b)
8	E_3	E_2	600	50	13(a) and 14(a)
9			500	40	13(b) and 14(b)

REFERENCES

- J. Jiménez, "Coherent structures in wall-bounded turbulence," *J. Fluid Mech.* **842**, P1 (2018).
- M. Tlidi, P. Mandel, and M. Haelterman, "Spatiotemporal patterns and localized structures in nonlinear optics," *Phys. Rev. E* **56**, 6524–6530 (1997).
- P. Parra-Rivas, E. Knobloch, L. Gelens, and D. Gomila, "Origin, bifurcation structure and stability of localized states in Kerr dispersive optical cavities," *IMA J. Appl. Math.* **86**, 856–895 (2021).
- S. Ramaswamy, "The mechanics and statistics of active matter," *Annu. Rev. Condens. Matter Phys.* **1**, 323–345 (2010).
- M. James, W. J. T. Bos, and M. Wilczek, "Turbulence and turbulent pattern formation in a minimal model for active fluids," *Phys. Rev. Fluids* **3**, 061101 (2018).
- P. Cvitanović, "Recurrent flows: The clockwork behind turbulence," *J. Fluid Mech.* **726**, 1–4 (2013).
- G. J. Chandler and R. R. Kerswell, "Invariant recurrent solutions embedded in a turbulent two-dimensional Kolmogorov flow," *J. Fluid Mech.* **722**, 554–595 (2013).
- C. J. Crowley, J. L. Pughe-Sanford, W. Toler, M. C. Krygier, R. O. Grigoriev, and M. F. Schatz, "Turbulence tracks recurrent solutions," *Proc. Natl. Acad. Sci. U.S.A.* **119**, 1–7 (2022).
- R. R. Kerswell, "Recent progress in understanding the transition to turbulence in a pipe," *Nonlinearity* **18**, R17–R44 (2005).
- B. Eckhardt, T. M. Schneider, B. Hof, and J. Westerweel, "Turbulence transition in pipe flow," *Annu. Rev. Fluid Mech.* **39**, 447–468 (2007).
- J. F. Gibson, J. Halcrow, and P. Cvitanović, "Visualizing the geometry of state space in plane Couette flow," *J. Fluid Mech.* **611**, 107–130 (2008).
- G. Kawahara, M. Uhlmann, and L. van Veen, "The significance of simple invariant solutions in turbulent flows," *Annu. Rev. Fluid Mech.* **44**, 203–225 (2012).
- B. Suri, J. Tithof, R. O. Grigoriev, and M. F. Schatz, "Forecasting fluid flows using the geometry of turbulence," *Phys. Rev. Lett.* **118**, 114501 (2017).
- M. D. Graham and D. Floryan, "Exact coherent states and the nonlinear dynamics of wall-bounded turbulent flows," *Annu. Rev. Fluid Mech.* **53**, 227–253 (2021).
- G. Kawahara and S. Kida, "Periodic motion embedded in plane Couette turbulence: Regeneration cycle and burst," *J. Fluid Mech.* **449**, 291–300 (2001).
- L. van Veen and G. Kawahara, "Homoclinic tangle on the edge of shear turbulence," *Phys. Rev. Lett.* **107**, 114501 (2011).
- B. Suri, R. K. Pallantla, M. F. Schatz, and R. O. Grigoriev, "Heteroclinic and homoclinic connections in a Kolmogorov-like flow," *Phys. Rev. E* **100**, 1–14 (2019).
- F. Reetz and T. M. Schneider, "Invariant states in inclined layer convection. Part 1. Temporal transitions along dynamical connections between invariant states," *J. Fluid Mech.* **898**, A22 (2020).
- C. E. P. De Jesús and M. D. Graham, "Data-driven low-dimensional dynamic model of Kolmogorov flow," *Phys. Rev. Fluids* **8**, 044402 (2023).
- C. Nore, L. S. Tuckerman, O. Daube, and S. Xin, "The 1:2 mode interaction in exactly counter-rotating von Kármán swirling flow," *J. Fluid Mech.* **477**, 51–88 (2003).
- A. J. Homburg and B. Sandstede, "Homoclinic and heteroclinic bifurcations of vector fields," in *Handbook of Dynamical Systems* 3, edited by H. Broer, F. Takens, and B. Hasselblatt (Elsevier, 2010), pp. 1–124.
- F. Reetz, P. Subramanian, and T. M. Schneider, "Invariant states in inclined layer convection. Part 2. Bifurcations and connections between branches of invariant states," *J. Fluid Mech.* **898**, A23 (2020).
- W.-J. Beyn, "The numerical computation of connecting orbits in dynamical systems," *IMA J. Numer. Anal.* **10**, 379–405 (1990).
- J. Halcrow, J. F. Gibson, P. Cvitanović, and D. Viswanath, "Heteroclinic connections in plane Couette flow," *J. Fluid Mech.* **621**, 365–376 (2009).
- P. Cvitanović, R. L. Davidchack, and E. Siminos, "On the state space geometry of the Kuramoto-Sivashinsky flow in a periodic domain," *SIAM J. Appl. Dyn. Syst.* **9**, 1–33 (2010).
- M. Farano, S. Cherubini, J.-C. Robinet, P. De Palma, and T. M. Schneider, "Computing heteroclinic orbits using adjoint-based methods," *J. Fluid Mech.* **858**, R3 (2019).
- Y. Liu, L. Liu, and T. Tang, "The numerical computation of connecting orbits in dynamical systems: A rational spectral approach," *J. Comput. Phys.* **111**, 373–380 (1994).
- C. Dong and Y. Lan, "A variational approach to connecting orbits in nonlinear dynamical systems," *Phys. Lett. Sect. A: Gen. At. Solid State Phys.* **378**, 705–712 (2014).
- Y. Lan and P. Cvitanović, "Variational method for finding periodic orbits in a general flow," *Phys. Rev. E* **69**, 016217 (2004).
- R. K. Pallantla, "Exact coherent structures and dynamical connections in a quasi 2D Kolmogorov like flow," Ph.D. thesis (Georgia Institute of Technology, 2018).
- M. Farazmand, "An adjoint-based approach for finding invariant solutions of Navier-Stokes equations," *J. Fluid Mech.* **795**, 278–312 (2016).
- S. Azimi, O. Ashtari, and T. M. Schneider, "Constructing periodic orbits of high-dimensional chaotic systems by an adjoint-based variational method," *Phys. Rev. E* **105**, 014217 (2022).
- J. P. Boyd, *Chebyshev and Fourier Spectral Methods* (Dover Publications, Inc., New York, 2001).
- Y. Kuramoto and T. Tsuzuki, "Persistent propagation of concentration waves in dissipative media far from thermal equilibrium," *Prog. Theor. Phys.* **55**, 356–369 (1976).
- G. I. Sivashinsky, "Nonlinear analysis of hydrodynamic instability in laminar flames—I. Derivation of basic equations," *Acta Astronaut.* **4**, 1177–1206 (1977).
- R. E. LaQuey, S. M. Mahajan, P. H. Rutherford, and W. M. Tang, "Nonlinear saturation of the trapped-ion mode," *Phys. Rev. Lett.* **34**, 391–394 (1975).
- A. P. Hooper and R. Grimshaw, "Nonlinear instability at the interface between two viscous fluids," *Phys. Fluids* **28**, 37–45 (1985).
- J. M. Hyman and B. Nicolaenko, "The Kuramoto-Sivashinsky equation: A bridge between PDE's and dynamical systems," *Phys. D* **18**, 113–126 (1986).
- Y. S. Smyrlis and D. T. Papageorgiou, "Computational study of chaotic and ordered solutions of the Kuramoto-Sivashinsky equation," Tech. Rep. (Institute for Computer Applications in Science and Engineering, NASA Langley Research Center, 1996).
- D. Rempfer, "On boundary conditions for incompressible Navier-Stokes problems," *Appl. Mech. Rev.* **59**, 107–125 (2006).
- J. P. Parker and T. M. Schneider, "Invariant tori in dissipative hyperchaos," *Chaos* **32**, 113102 (2022).
- J. P. Parker, O. Ashtari, and T. M. Schneider, "Predicting chaotic statistics with unstable invariant tori," *arXiv.2301.10626* (2023), pp. 1–11.